ORGANIC CHEMISTRY FRONTIERS

RESEARCH ARTICLE

View Article Online
View Journal | View Issue

Cite this: *Org. Chem. Front.*, 2026, **13**, 3763

Post-Ugi synthesis of furo[2,3-*c*]isoquinolines with expanded π-conjugation displaying emission upon induced aggregation

Tullio Crovetto,[a] Lukas Biesen,[b] Andrea Messina,[a] Lisa Moni,[a] Chiara Lambruschini,[a] Bernhard Mayer,[b] Thomas J. J. Müller *[b] and Renata Riva *[a]

Received 11th March 2026,
Accepted 23rd April 2026

DOI: 10.1039/d6qo00311g

rsc.li/frontiers-organic

Furo[2,3-*c*]isoquinolines are tricyclic heteroaromatic structures that can be obtained by coupling the Ugi reaction with a complex Pd-mediated secondary transformation. These compounds are usually blue emitters, which can be converted to green emitters by modulating the electronic properties of the substituents as well as their position on the scaffold. Here, we present a different strategy for tuning the emission properties, which is the extension of the conjugation of the scaffold after the formation of the tricyclic heterocycle. This allowed us to synthesize a new library of highly conjugated and structurally complex fluorophores displaying considerable emission light-up upon induced aggregation. The electronic structure of absorption and emission of the chromophores was rationalized by cLR-CAM-B3LYP calculations.

Introduction

The continuously increasing demand for functional molecules and materials with novel properties[1–3] is particularly evident in the field of functional dyes,[4] which underpin a wide range of photonic and electronic applications.[5–7] Control of function through structural variation[8,9] is often closely linked to aggregation processes, *i.e.*, the transition from solution to the solid state.[10–12] Aggregation-induced emission (AIE)[13–16] and aggregation-induced enhanced emission (AIEE)[17,18] provide a versatile framework, in which induced aggregation of fluorophores leads to emission behaviours ranging from turn-on to substantial luminescence enhancement, thereby enabling fine control over material properties.[19,20] These effects are commonly rationalized by the suppression of nonradiative decay pathways, arising from the restriction of intramolecular motions (RIM)[21,22] or restricted access to conical intersections (RACI).[23,24]

Aggregation-modulated emission properties have opened numerous opportunities for luminescent functional dyes, particularly in photonic applications (*e.g.*, photovoltaics and OLEDs)[25–28] as well as in biomedical applications,[29,30] analytical science,[31,32] and sensing.[33,34] Notably, many such functional dyes have traditionally been accessed through classical multistep synthetic approaches. However, these challenges can also be addressed through diversity-oriented synthetic strategies, which enable the efficient and concise assembly of functional π-conjugated molecules *via* one-pot methodologies, such as multicomponent reactions (MCRs).[35–37] In this context, transition metal-catalyzed sequences have proven especially powerful for the MCR-based synthesis of fluorophores.[38,39] In particular, solid-state and aggregation-induced emissive chromophores have been successfully realized using metal-catalyzed MCR strategies.[40]

Post-Ugi transformations, which capitalize on the rapid generation of structurally diverse substrates for heterocycle synthesis, frequently involve metal-mediated cascade processes.[41,42] In our initial studies, a consecutive Ugi four-component reaction (Ugi-4CR) followed by reductive Heck cyclization enabled efficient access to highly substituted, blue-emissive 3-hydroxyisoquinolines.[43] Further development of this strategy, incorporating alkynylation, culminated in a domino Heck cyclization–Sonogashira coupling–cyclization sequence, affording tricyclic furo[2,3-*c*]isoquinolines of general structure **2** starting from **1** (1st generation, Scheme 1).[44]

These compounds exhibited pronounced tunability of blue emission and fluorescence quantum yields, which are influenced by the structure of the substituents R^1–R^4, especially when R^2 and/or R^4 are donors. On the other hand, substituents R^5 and R^6 do not significantly influence the emission, due to the lack of conjugation with the heteroaromatic scaffold.

These properties could be further modulated and enhanced through different donor substituents at C_1 and/or C_8 of the

[a]*Dipartimento di Chimica e Chimica Industriale, Università di Genova, Via Dodecaneso, 31, 16166 Genova, Italy. E-mail: renata.riva@unige.it*
[b]*Institut für Organische Chemie und Makromolekulare Chemie, Heinrich-Heine-Universität Düsseldorf, Universitätsstraße 1, 40225 Düsseldorf, Germany. E-mail: ThomasJJ.Mueller@uni-duesseldorf.de*

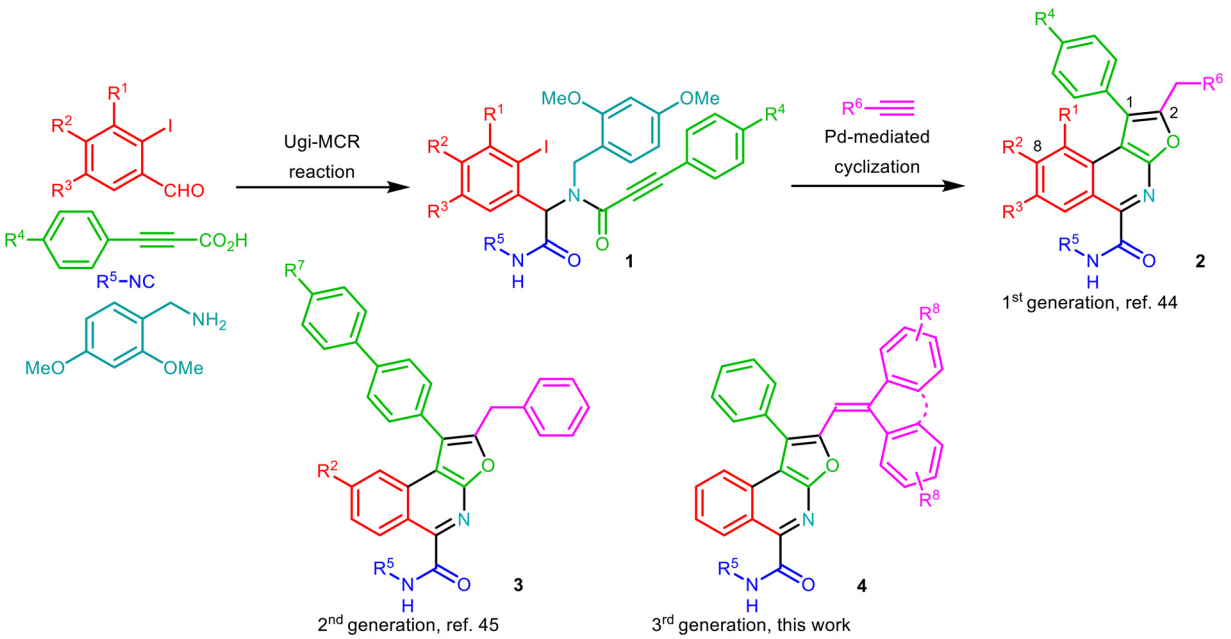

Scheme 1 Summary of the development of the project to ensure a bathochromic effect in the emission wavelength.

heterocyclic core (compound **3** is one of the possible generic structures we studied in the 2nd generation of molecules).[45] In particular, an amino donor on C_8 caused a significant switch to green emitters. The biaryl substituent at C_1, instead, has almost no influence on the emission, which is due, at least in part, to the incomplete coplanarity with the furoisoquinoline scaffold, as demonstrated by DFT calculations.[45]

To extend the luminescent furo[2,3-*c*]isoquinoline scaffold toward more red-shifted emissive luminophores, we explored a different strategy to expand the π-conjugation, which was suggested by the benzyl substituent on C_2 (R^6 = Ar in structure **2**). For this purpose, we planned to introduce a double bond-forming elimination step following the cyclization cascade. Herein, we report the synthetic and methodological development of *gem*-diphenyl-ethenylene-substituted furo[2,3-*c*]isoquinolines and fluorenylidene furo[2,3-*c*]isoquinolines, together with an investigation of their photophysical properties. Emission behavior in solution, in the solid state, and under induced aggregation conditions is examined, and the underlying electronic structures are rationalized using TD-DFT calculations.

Results and discussion

Chemistry

Going into greater detail on the highly convergent synthetic strategy, we started with a Ugi multicomponent reaction (MCR) employing 2-iodobenzaldehyde, propiolic acid, an isocyanide, and 2,4-dimethoxybenzyl (DMB) amine as an ammonia synthetic equivalent to afford **1**. Then, we performed the one-pot Pd-mediated domino procedure with the inclusion of a terminal alkyne (Scheme 1).

This complex sequence, which we called **HSCA**, is illustrated in Scheme 2 on a specific Ugi product (**1a**, R^5 = *t*-Bu) and is the result of an intramolecular **H**eck coupling, where intermediate **5** undergoes a copper-free **S**onogashira reaction with the terminal alkyne to afford a mixture of diastereomeric alkenes (***Z*)-6** and (***E*)-6**, probably due to a poorly stereoselective Heck reaction. The former spontaneously undergoes **C**yclo**A**romatization, after the *in situ* cleavage of the DMB group, and affords **2** as the main product, while (***E*)-6**, unable to cyclize for geometrical reasons, was recovered as it was. We found that, to exploit both (***Z*)-** and (***E*)-6**, the addition of 1,8-diazabicyclo[5.4.0]undec-7-ene (DBU) promotes a reversible isomerization of (***E*)-6** to (***Z*)-6**, allowing the complete transformation of **6** into **2**.[44]

The strategy for expanding the π-conjugation is highlighted in the retrosynthetic plan (Scheme 3). General structure **4** can, in principle, be obtained if a methyl propargyl ether such as **8** is used as the terminal alkyne in the HSCA sequence, transforming Ugi product **1** into **7**.

The advantages of using **8** are as follows: (a) OMe is a possible leaving group in the β-elimination, responsible for the conjugation enhancement; (b) propargylic C is quaternary, which considerably affects the yield of the HSCA, affording **7**;[44] and (c) the possibility of decorating the scaffold with different substituents (groups R^8 with electron-donating or electron-withdrawing properties), and different connections between the two aromatic rings (dashed curve).

All compounds **8** required a specific, usually multistep, synthesis. Moreover, we aimed to design efficient strategies possibly based on common intermediates. The synthetic planning, as well as the issues encountered, is described in the SI, while in Scheme 4, all the structures of compounds **8** are reported.

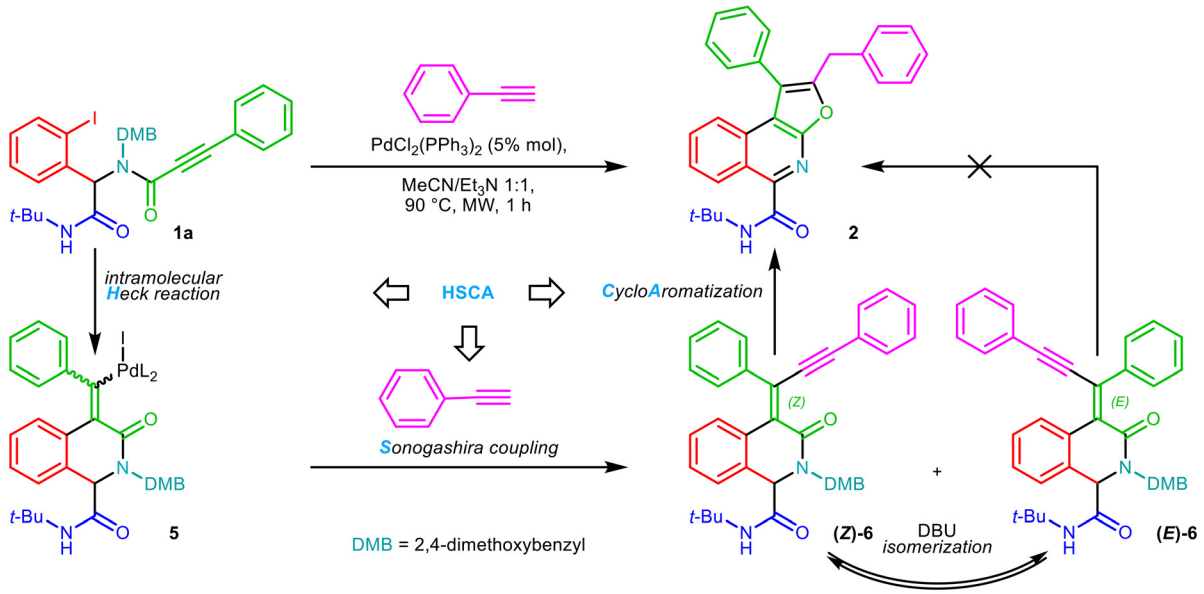

Scheme 2 The possible mechanistic rationale of the Heck–Sonogashira-cycloaromatization (HSCA) sequence.

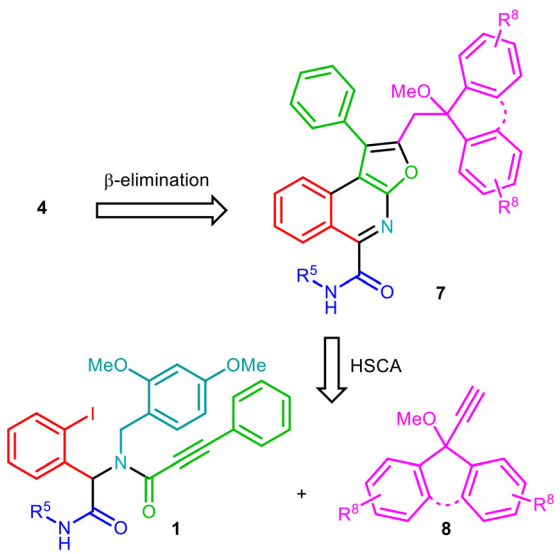

Scheme 3 Retrosynthetic plan.

As mentioned earlier, the aim of the project was to study the influence of alkyne **8** on the photophysical properties of **4**. For this reason, we did not explore the diversity of the components in the Ugi reaction, with just one exception, represented by the isocyanide. Knowing that the secondary amide arising from the isocyanide (compound **1**, Scheme 3) does not significantly affect the photophysical properties, we decided to keep the structure of R^5 fixed as *t*-Bu, using *t*-BuNC in the Ugi reaction. However, in some cases, the *t*-Bu group was cleaved under the conditions of β-elimination (see below), affording the primary amide (R^5 = H). For this reason, in some instances, we used *n*-BuNC (R^5 = *n*-Bu) as the isocyanide.

The two Ugi products (**1a** R^5 = *t*-Bu and **1b** R^5 = *n*-Bu, Table 1) used as starting materials were synthesized as previously reported in 85% and 95% yields, respectively.[43]

We therefore focused on the previously optimized Pd-mediated transformation[44] of **1a** into **7a** (Table 1, entry 1), but we observed the formation of two compounds, namely a mixture of **7a** and **4a**. This indicates a strong tendency of **7a** toward elimination, but the reaction did not go to completion even upon MW-heating after the addition of more DBU, the base used for the isomerization of **(*E*)-6** to **(*Z*)-6**. We eventually found that, after work-up of the crude mixture, followed by fast filtration over silica gel, the transformation of **7a** into **4a** could be driven to completion by treatment with *p*-toluenesulfonic acid (*p*-TSA) in refluxing chloroform.

Nevertheless, the β-elimination turned out to be a crucial step that required customized conditions optimized for the synthesis of each compound **4** from the corresponding **7**.

In most cases (entries 1, 2, 5–8 and 10–12), the conditions of choice were very similar to the ones described above, with the largest differences in reaction time and the number of MW-heating cycles in the presence of additional DBU, before adding *p*-TSA. The exact conditions for each compound are reported in the Experimental section (see the SI).

A significant difference was observed when **8c** was used as the terminal alkyne in the HSCA sequence involving Ugi derivative **1a** (entry 3). In this case, treatment with *p*-TSA in refluxing chloroform did not promote the β-elimination at all. For this reason, we switched to toluene as the solvent, and the mixture was heated to reflux. This time, the transformation was accomplished smoothly. However, the harsh conditions used also promoted the cleavage of the *t*-Bu group, and we isolated the primary amide **4c$_1$** (R^5 = H) starting from **7c$_1$** (R^5 = *t*-Bu). Therefore, we repeated the whole sequence starting from Ugi

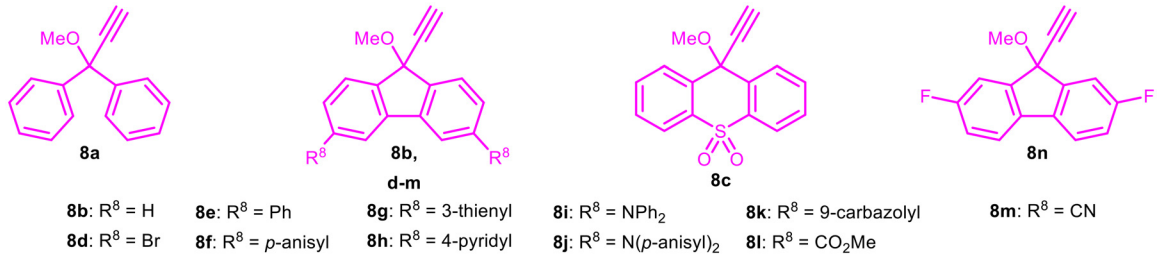

Scheme 4 Structure of terminal alkynes **8a–n**.

Table 1 Synthesis of the library of compounds **4a–n**

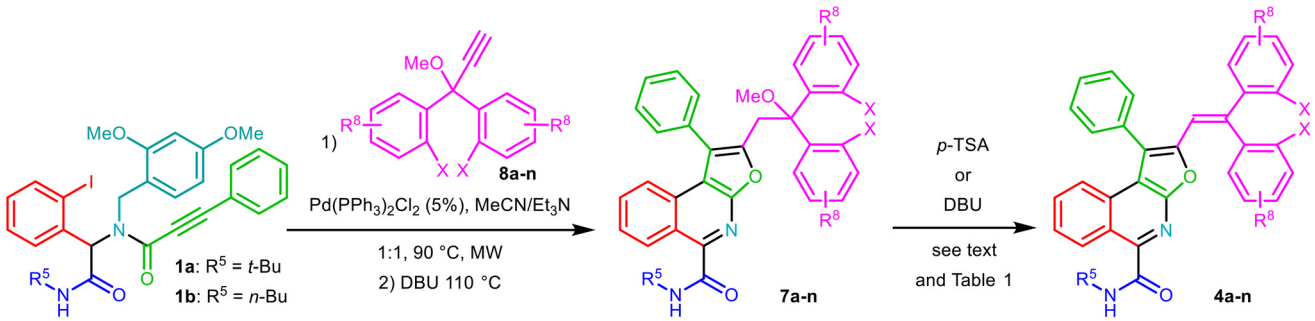

Entry	R^5 (Ugi product)	Alkyne	Elimination method[a,b]	Product	Yield (HSCA + β-elimination)[c]
1	*t*-Bu (**1a**)	**8a** (X = H,H, R^8 = H)	DBU, then *p*-TSA	**4a**	54%
2	*t*-Bu (**1a**)	**8b** (X = —, R^8 = H)	DBU, then *p*-TSA	**4b**	62%
3	*t*-Bu (**1a**)	**8c** (X = SO_2, R^8 = H)	DBU, then *p*-TSA	**4c$_1$** (R^5 = H)	69%
4	*n*-Bu (**1b**)	**8c** (X = SO_2, R^8 = H)	DBU, then *p*-TSA	**4c$_2$** (R^5 = *n*-Bu)	47%
5	*t*-Bu (**1a**)	**8d** (X = —, R^8 = Br)	DBU, then *p*-TSA	**4d**	23%
6	*t*-Bu (**1a**)	**8e** (X = —, R^8 = Ph)	DBU, then *p*-TSA	**4e**	54%
7	*t*-Bu (**1a**)	**8f** (X = —, R^8 = *p*-anisyl)	DBU, then *p*-TSA	**4f**	42%
8	*t*-Bu (**1a**)	**8g** (X = —, R^8 = 3-thienyl)	DBU, then *p*-TSA	**4g**	52%
9	*t*-Bu (**1a**)	**8h** (X = —, R^8 = 4-pyridyl)	DBU	**4h**	69%
10	*t*-Bu (**1a**)	**8i** (X = —, R^8 = NPh_2)	DBU, then *p*-TSA	**4i**	58%
11	*t*-Bu (**1a**)	**8j** (X = —, R^8 = $N(p\text{-anisyl})_2$)	DBU, then *p*-TSA	**4j**	50%
12	*t*-Bu (**1a**)	**8k** (X = —, R^8 = 9-carbazolyl)	DBU, then *p*-TSA	**4k**	75%
13	*n*-Bu (**1b**)	**8l** (X = —, R^8 = CO_2Me)	DBU	**4l**	77%
14	*n*-Bu (**1b**)	**8m** (X = —, R^8 = CN)	DBU	**4m**	61%
15	*t*-Bu (**1a**)	**8n** (X = —, R^8 = F)	DBU	**4n**	53%

[a] This column reports only the main reagent; further details can be found in the text and in the SI. [b] The elimination was performed on compounds **7a–n** affording **4a–n**. However, in case of **7c$_1$** (R^5 = *t*-Bu) and **7c$_2$** (R^5 = *n*-Bu), the elimination afforded **4c$_1$** (R^5 = H) and **4c$_2$** (R^5 = *n*-Bu), respectively (see text for more details). [c] From Ugi product (**1a** or **1b**).

product **1b** (entry 4). Once again, the β-elimination required the most severe conditions to proceed, but this time, we isolated the expected furo[2,3-*c*]isoquinoline, which we called **4c$_2$** (R^5 = *n*-Bu). Only in a few cases (entries 9 and 13–15), the β-elimination was complete by further addition of exclusively DBU and MW-heating after completion of the HSCA.

For the synthesis of compounds **4l,m**, we decided to start from **1b**, concerned that the presence of electron-withdrawing substituents at positions 3,6 of the (9-methoxy-9*H*-fluoren-9-yl) methyl moiety (**8l,m**) might account for the harsher conditions necessary for the β-elimination on the 10,10-dioxi-do-9*H*-thioxantene-derived **7c$_1$** and **7c$_2$** with an electron-withdrawing sulfone moiety. For both compounds, the HSCA was slower, but in this case, the β-elimination could be performed using DBU only.

For **8n**, with two fluorine atoms at positions 2 and 7 (entry 15), once again, the HSCA and the β-elimination were very slow. We eventually were able to drive the reaction to completion after isolating the mixture of **7n** and **4n** and treating it under MW heating at 110 °C in MeCN in the presence of additional DBU. In contrast, the β-elimination under acidic conditions did not work at all.

The overall yield of this procedure was good, considering the complexity of the transformation, with the only exception represented by **4d**, most likely due to the limited compatibility of the bromine atom with Pd-catalysis. This is the reason why we decided not to use **4d** as an advanced intermediate for functionalization at positions 3 and 6, as discussed in the SI.

Photophysical properties and electronic structure of fluoren-9-ylidene-furo[2,3-*c*]isoquinolines 4

Longest wavelength absorption maxima for compounds **4** in 1,4-dioxane appear as intense bands in a range from 398 to 513 nm with molar extinction coefficients ε between 20 900 and 45 900 L mol^{-1} cm^{-1} (Table 2).

The emission maxima in 1,4-dioxane ($\lambda_{exc} = \lambda_{max,abs}$) are found in a range from 489 to 683 nm with fluorescence quantum yields Φ_F between 0.01 and 0.16 (Fig. 1). Only compound **4n** does not exhibit any emission upon photonic excitation. The Stokes shifts fall in a margin between 2500 and 4800 cm^{-1} and indicate only minor structural changes between the ground state and vibrationally relaxed excited state upon photonic excitation. The emission maxima in the solid state are red-shifted and appear, with the exception of dyes **4i** and **4j**, in a range between 496 and 636 nm and with fluorescence quantum yields Φ_F between 0.02 and 0.22, similar to those in solution (Fig. 2, Table 2). In general, the quantum yields for dyes with Stokes shifts exceeding 4000 cm^{-1} are higher, which can be attributed to diminished competitive self-absorption. Any attempts to establish structure–property relationships for the consanguineous series of fluorenylidene dyes **4b**, **4d–4m** with remote substituents R^8 in conjugation to the extended π-conjugation of the furo[2,3-*c*] isoquinolines were inefficacious. The fact that $\lambda_{max,abs}$ (447 nm) and $\lambda_{max,em}$ (517 nm) of the unsubstituted dye **4b** represent the highest excitation and emission energies indicates a rather complex electronic structure of photonic excitation.

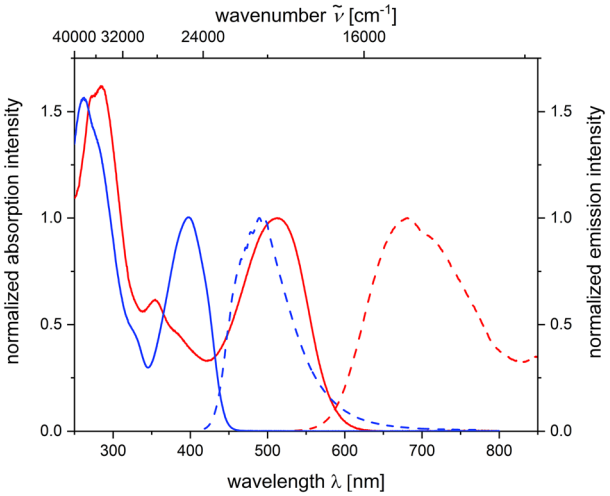

Fig. 1 Normalized absorption (solid) and emission (dashed) spectra of representative dyes **4a** (highest absorption and emission energies, in blue) and **4j** (lowest absorption and emission energies, in red) (recorded in 1,4-dioxane; abs: c(**4a**/**4j**) = 10^{-5} M; em: c(**4a**/**4j**) = 10^{-7} M; at T = 293 K, λ_{exc}(**4a**/**4j**) = λ_{max}(**4a**/**4j**)).

For rationalizing the electronic structure underlying the absorption spectra and the nature of the longest wavelength absorption bands, we chose a similar approach to that used for the previously reported 2nd generation of furo[2,3-*c*]isoquinoline fluorophores.[45] DFT and TD-DFT calculations are carried out using the program package of Gaussian 16[46] with various DFT functionals (B3LYP, CAM-B3LYP, and LC-ωB97XD)[47–51] and

Table 2 Selected photophysical properties (absorption $\lambda_{max,abs}$, molar decadic extinction coefficient ε, emission maximum $\lambda_{max,em}$, fluorescence quantum yield Φ_f, Stokes shift in solution, and emission maximum $\lambda_{max,em}$ and fluorescence quantum yield Φ_f in the solid state) of fluoren-9-ylidene-furo[2,3-*c*]isoquinolines **4**

Entry	Compound	$\lambda_{max,abs}$ solution [nm] (ε [L mol^{-1} cm^{-1}])[a]	$\lambda_{max,em}$ solution [nm][b] (Φ_f)	Stokes shift $\Delta\tilde{\nu}$[c] [cm^{-1}]	$\lambda_{max,em}$ solid state [nm] (Φ_f)[d]
1	**4a** (X = H,H, R^8 = H)	263 (44 000), 398 (27 400)	489 (0.16)	4700	496 (0.18)
2	**4b** (X = —, R^8 = H)	267(42 200), 274 (32 500), 339 (8300), 425 (23 400), 447 (20 900)	517 (<0.01)	3000	591 (0.07)
3	**4c$_1$** (X = SO$_2$, R^8 = H, R^5 = *t*-Bu)	339 (6700), 409 (16 400)	496 (<0.01)	4300	513 (0.03)
4	**4c$_2$** (X = SO$_2$, R^8 = H, R^5 = *n*-Bu)	338 (15 700), 410 (36 600)	499 (0.01)	4400	537 (0.16)
5	**4d** (X = —, R^8 = Br)	279 (56 000), 346 (18 300), 444 (50 600), 468 (45 900)	534 (0.01)	2600	594 (0.02)
6	**4e** (X = —, R^8 = Ph)	262 (31 900), 272 (29 400), 284 (10 000), 346 (10 000), 435 (28 400), 458 (25 900)	518 (0.01)	2500	622 (0.22)
7	**4f** (X = —, R^8 = *p*-anisyl)	268 (37 000), 351 (11 700), 449 (29 100)	548 (0.01)	4000	620 (0.03)
8	**4g** (X = —, R^8 = 3-thienyl)	272 (37 800), 349 (11 800), 447 (31 300), 472 (25 900)	545 (0.01)	2800	600 (0.03)
9	**4h** (X = —, R^8 = 4-pyridyl)	278 (70 300), 345 (14 400), 444 (42 200), 468 (39 100)	533 (0.01)	3800	610 (0.05)
10	**4i** (X = —, R^8 = NPh$_2$)	280 (43 300), 343 (23 100), 486 (32 000)	612 (0.14)	4300	—
11	**4j** (X = —, R^8 = *N*(*p*-anisyl)$_2$)	285 (47 400), 355 (18 300), 513 (29 100)	683 (0.03)	4800	—
12	**4k** (X = —, R^8 = 9-carbazolyl)	258 (96 300), 291 (55 900), 326 (24 200), 340 (25 300), 451 (44 200)	554 (0.08)	4100	608 (0.03)
13	**4l** (X = —, R^8 = CO$_2$Me)	264 (87 300), 344 (9400), 444 (33 700), 468 (32 500)	538 (0.01)	2800	623 (0.08)
14	**4m** (X = —, R^8 = CN)	263 (57 900), 345 (5900), 450 (22 400), 472 (21 300)	539 (0.01)	2600	636 (0.07)
15	**4n** (X = —, R^8 = F)	265 (43 700), 338 (14 100), 426 (43 300), 447 (40 100)	—	—	—

[a] Recorded in 1,4-dioxane, T = 298 K, c(**4**) = 10^{-5} M. [b] Recorded in 1,4-dioxane, T = 298 K, c(**4**) = 10^{-7} M, $\lambda_{exc} = \lambda_{abs,max}$, if not specified otherwise. [c] $\Delta\tilde{\nu} = \tilde{\nu}_{max,abs} - \tilde{\nu}_{max,em}$ [cm^{-1}]. [d] Recorded in an integrating sphere, T = 298 K, $\lambda_{exc} = \lambda_{abs,max}$.

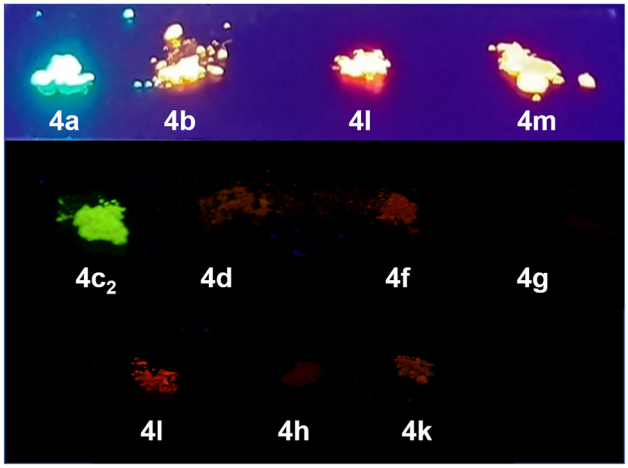

Fig. 2 Solid-state emission of selected dyes **4** under a hand-held UV lamp (λ_{exc} = 365 nm).

Pople's 6-31+G** basis set[52] employing the corrected linear response (cLR) model for implementing a state specific solvent response.[53] The polarizable continuum model (PCM) for 1,4-dioxane as a solvent[54] is chosen to allow a comparison between calculated and experimentally determined optical transitions. TD-DFT calculations were performed using exchange–correlation functionals B3LYP, CAM-B3LYP, and LC-ωB97XD to assess the impact of exchange treatment on excitation energies, as global hybrids like B3LYP can underestimate long-range charge-transfer contributions, while range-separated hybrids improve asymptotic exchange behavior.[55–57] The functionals were benchmarked against experimental absorption and emission maxima, providing a physically meaningful validation since these energies are observable quantities.[58–60]

First, the geometries of the electronic ground-state structures of selected fluoren-9-ylidene-furo[2,3-*c*]isoquinolines (**4b**, **4k**, and **4m**) and the *gem*-diphenyl ethenylene furo[2,3-*c*]isoquinoline **4a** are optimized and all minimum structures are unambiguously confirmed by analytical frequency analyses. While cLR-TD-DFT calculations with CAM-B3LYP and LC-ωB97XD functionals underestimate the lowest energy absorption bands in comparison to B3LYP, CAM-B3LYP consistently gives the smallest $\Delta E_{calcd\text{-}exp}$ in a range from 0.1728 to 0.2939 eV, and concomitantly high oscillator strengths are well aligned with intense π–π* (LE) transitions with no indication of strongly long-range charge-transfer character. In the consanguineous series of fluorenylidene dyes **4b** (exp: 447 nm; calcd: 409 nm), **4k** (exp: 451 nm; calcd: 421 nm), and **4m** (exp: 472 nm; calcd: 425 nm), the trend of the unsubstituted dye **4b** with the highest absorption energy and the lower absorption energies of the bis(*N*-carbazolyl) substituted dye **4k** and the biscyano substituted dye **4m** in the experimental spectra is nicely reproduced by the calculations (Table 3, Table S3).

Most characteristically for all four calculated structures **4b**, **4k**, **4m**, and **4a**, the absorption and emission bands of the dyes originate from HOMO–LUMO transitions with intense LE (locally excited) character (Table 3, Fig. 3). The Kohn–Sham FMOs reveal dominant coefficient density on the fluoren-9-ylidene-furo[2,3-*c*]isoquinoline or *gem*-diphenyl ethenylene furo[2,3-*c*]isoquinoline part, respectively. Coefficient density on the unsubstituted dye **4a** is significant at the position of substitution in both HOMO and LUMO. Therefore, substitution can be expected to exert a minor impact on the absorption spectra, as seen for both the experimental and calculated spectra. The direct comparison between fluoren-9-ylidene-furo[2,3-*c*]isoquinoline **4b** and *gem*-diphenyl ethenylene furo[2,3-*c*]isoquinoline **4a** additionally reveals the extended π-conjugation exerted by the fluorenylidene causing, as expected, a clear redshift of the absorption band of dye **4b** with respect to **4a**.

Moreover, the same cLR-DFT functional CAM-B3LYP is used for implementing a state specific solvent response to calculate the emission spectra of dyes **4b**, **4k**, **4m**, and **4a**, which is then employed for modelling the excitation–relaxation–emission–relaxation cycles for dyes **4a** and **4b** (Fig. 4). The emission spectra are reproduced reasonably well by the TD-DFT calculations and also the Stokes shifts of calculated and experimental spectra fall into a similar region.

Table 3 Selected experimental and TD-DFT calculated (absorption: cLR-DFT functional CAM-B3LYP; basis set 6-31+G**; emission: state-specific-DFT functional CAM-B3LYP; basis set 6-31+G**) first excited singlet states of the consanguineous dyes fluoren-9-ylidene-furo[2,3-*c*]isoquinolines **4b**, **4k**, **4m**, and *gem*-diphenyl ethenylene furo[2,3-*c*]isoquinoline **4a** in 1,4-dioxane as an extrinsic dielectric using the polarizable continuum model (PCM)

		Exp	Calcd (f)	$\Delta E_{calcd\text{-}exp}$ [eV]	Dominant transition
4b	$\lambda_{max,abs}$ [nm]	447	408.9 (1.2437)	0.2583	HOMO → LUMO (95.7%)
	Emission [nm]	517	496.4 (1.0833)	0.0992	HOMO → LUMO (98.2%)
	Stokes shift [cm^{-1}]	3000	4300		
4k	Absorption [nm]	451	420.6 (1.5054)	0.1984	HOMO → LUMO (71.9%)
	Emission [nm]	554	520.2 (1.3628)	0.1452	HOMO → LUMO (93.6%)
	Stokes shift [cm^{-1}]	4100	4600		
4m	Absorption [nm]	472	424.5 (1.4051)	0.2940	HOMO → LUMO (95.8%)
	Emission [nm]	539	515.0 (1.1930)	0.1069	HOMO → LUMO (98.1%)
	Stokes shift [cm^{-1}]	2600	4100		
4a	Absorption [nm]	398	377.1 (1.0363)	0.1728	HOMO → LUMO (93.9%)
	Emission [nm]	489	490.0 (0.9138)	0.0052	HOMO → LUMO (97.7%)
	Stokes shift [cm^{-1}]	4700	6100		

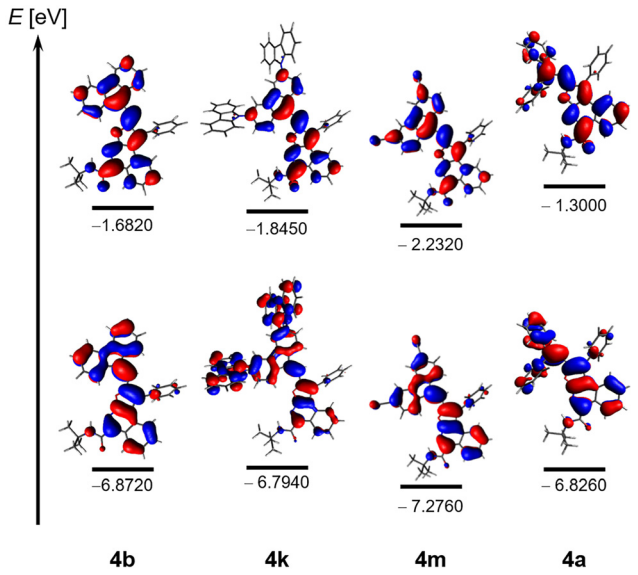

Fig. 3 Kohn–Sham FMOs of fluoren-9-ylidene-furo[2,3-*c*]isoquinolines (**4b**, **4k**, and **4m**) and the *gem*-diphenyl ethenylene furo[2,3-*c*]isoquinoline **4a** (calculated at the cLR-TD-DFT level of theory using CAM-B3LYP/6-31+G(d,p) including the PCM for 1,4-dioxane as a solvent dielectric).

While the quantum yields in solution are, with the exception of dyes **4a** (0.16), **4i** (0.14), and **4k** (0.08), rather low; however, they are quite substantial in the solid state (up to 0.22 for dye **4e**), except for strongly donor-substituted fluoren-9-ylidene-furo[2,3-*c*]isoquinolines **4i** and **4j**, the possibility of emission upon induced aggregation, also known as aggregation-induced emission (AIE), comes to mind.

AIE properties of dyes 4

All dyes **4** consist of quite rigid extended π-conjugated structures, and expectedly, their solubility in water is low. Therefore, for most dyes, upon increasing the water fraction f_w in 1,4-dioxane solutions, aggregation is induced, as can be seen by a light-up of green to orange emission upon UV excitation (Fig. 5, Table 4).

Since most of the dyes **4** are already emissive, often with low intensity, in 1,4-dioxane solution, with the exception of dyes **4b** and $\mathbf{4c_1}$, the fractional increase of the water content causes aggregation-induced emission enhancement. The emission enhancement can be quite substantial, especially for those dyes that are essentially non-emissive to the naked eye in solution

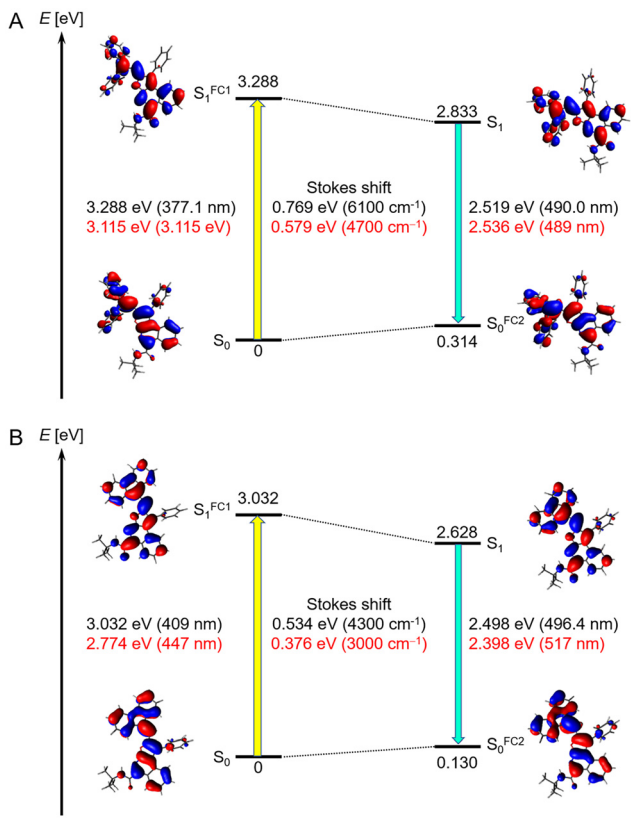

Fig. 4 Calculated excitation–relaxation–emission–relaxation cycles and most relevant frontier molecular orbitals for the Franck–Condon absorption ($S_0 \rightarrow S_1^{FC1}$) and emission ($S_0^{FC2} \leftarrow S_1$) of *gem*-diphenyl ethenylene furo[2,3-*c*]isoquinoline **4a** (A) and fluoren-9-ylidene-furo[2,3-*c*]isoquinoline **4b** (B) at the cLR-CAM-B3LYP/6-31+G(d,p) level of theory (including the PCM for 1,4-dioxane as a solvent dielectric).

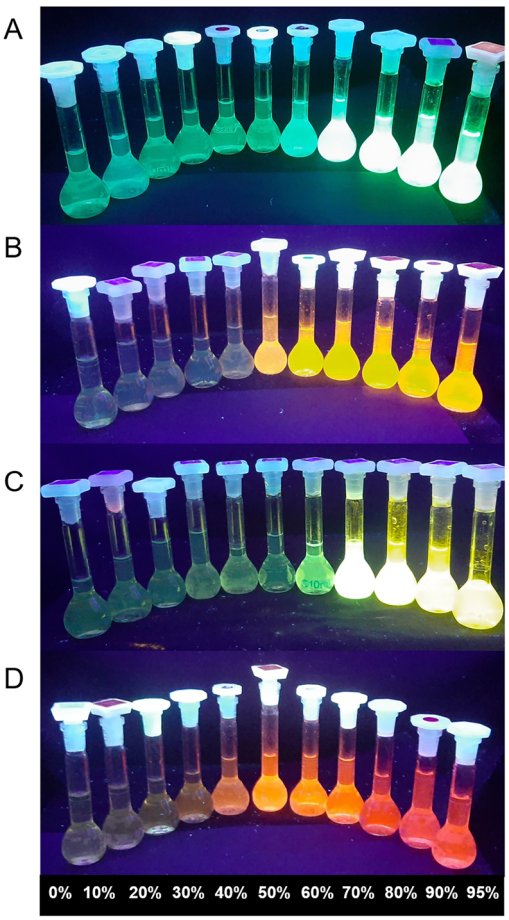

Fig. 5 Visualization (photographs) of the AIE features of selected dyes **4a** (A), **4b** (B), $\mathbf{4c_2}$ (C), and **4m** (D) in 1,4-dioxane/water mixtures of increasing water content (water fraction, f_w, given in %) upon excitation with a UV lamp ($c(\mathbf{4}) = 10^{-7}$ M, λ_{exc} = 365 nm).

Table 4 Emission data of selected dyes **4** in solution (1,4-dioxane), in the solid state, and upon induced aggregation (water fractions f_w in 1,4-dioxane solutions range from 0 to 95%) (recorded in an integrating sphere, T = 298 K, $\lambda_{exc} = \lambda_{abs,max}$)

Dye	Solution $\lambda_{max,em}$ ($\Phi_{f,max}$)	Solid state $\lambda_{max,em}$ ($\Phi_{f,max}$)	Emission upon induced aggregation $\lambda_{max,em}$ ($\Phi_{f,max}$), f_w@$\Phi_{f,max}$
4a	489 (0.16)	496 nm (0.18)	488.2 nm (0.59), f_w = 70%
4b	517 (<0.01)	591 nm (0.07)	587.4 nm (0.07), f_w = 60%
4c$_1$	496 (<0.01)	513 nm (0.03)	529.2 nm (0.15), f_w = 90%
4c$_2$	499 (0.01)	537 nm (0.16)	518.4 nm (0.28), f_w = 70%
4d	534 (0.01)	594 nm (0.02)	595.4 nm (0.08), f_w = 40%
4e	518 (0.01)	622 nm (0.22)	519.4 nm (0.02), f_w = 20%[a]
4f	548 (0.01)	620 nm (0.03)	606.2 nm (0.11), f_w = 50%
4g	545 (0.01)	600 nm (0.03)	558.4 nm (0.02), f_w = 30%[b]
4h	533 (0.01)	610 nm (0.05)	606 nm (0.09), f_w = 50%
4k	554 (0.08)	608 nm (0.03)	594.8 nm (0.12), f_w = 30%[c]
4l	538 (0.01)	623 nm (0.08)	644.8 nm (0.11), f_w = 60%
4m	539 (0.01)	636 nm (0.07)	632 nm (0.10) f_w = 60%

[a] An additional intensity maximum is found at 600 nm ($\Phi_{f,max}$ = 0.017), f_w = 50%. [b] An additional intensity maximum is found at 622.4 ($\Phi_{f,max}$ = 0.014), f_w = 50%. [c] An additional intensity maximum is found at 623.4 nm ($\Phi_{f,max}$ = 0.04), f_w = 80%.

(dyes **4b** and **4c$_2$**). The emission spectra of the aggregate solution at the maximum quantum yield quite nicely underline that these emission bands fall into the same energy range as for the solid-state maxima. Therefore, the molecules in the initial aggregates already adopt similar orientations to those in the solid state. However, in two cases (dyes **4e** and **4g**) where the emission band of AIEE is closer to the solution emission, additional bands arise from coagulation, which mostly coincides with the emission band maxima of the corresponding solid-state spectra. The comparison of the emission behavior of induced aggregation of the parent compound of fluoren-9-ylidene-furo[2,3-*c*]isoquinoline **4b** with the unlocked, more dynamic *gem*-diphenyl ethenylene furo[2,3-*c*]isoquinoline **4a** clearly reveals the difference between AIE (**4b**) and AIEE (**4a**).

Upon aggregation, the 30-fold emission enhancement of **4b** compared to solution can be seen as a turn-on of luminescence, whereas for dye **4a**, which already displays significant emission ($\Phi_{f,max}$ = 0.16) in pure 1,4-dioxane, the green emission enhancement boosts up to $\Phi_{f,max}$ = 0.59 at f_w = 70%. This can also be seen by the bright emission in the volumetric flask. The latter dye, **4a**, is suitable for designing AIEE dyes, which display considerably enhanced emission, whereas fluoren-9-ylidene-furo[2,3-*c*]isoquinolines **4b–m** can be considered as turn-on AIE dyes with tunable emission color from green over yellow to orange red.

Conclusions

In conclusion, we optimized a robust methodology for the preparation of a library of highly conjugated and structurally complex furo[2,3-*c*]isoquinolines in just three steps: a Ugi multicomponent reaction to afford a peptide framework endowed with two additional functional groups involved in complex Pd-mediated cyclization upon addition of a terminal alkyne with a leaving group in the propargylic position and finally β-elimination enabling connection of the furoisoquinoline scaffold with a highly conjugated aromatic moiety.

Furo[2,3-*c*]isoquinolines with extended π-conjugation by *gem*-diphenyl ethenylene or fluorenylidene substitution all display redshifted absorption bands in comparison with previously reported core substituted furo[2,3-*c*]isoquinolines. The lowest energy absorption bands can be predominantly assigned to intense π–π* (LE) transitions by TD-DFT calculations. In addition, the title compounds also display distinct bathochromically shifted luminescence, which can be seen as greenish to yellowish to orange-red emission with variable intensity.

Although only a few fluorenylidene-expanded furo[2,3-*c*]isoquinoline dyes exhibit substantial fluorescence quantum yield and most other congeners only emit very weakly, almost all dyes are highly luminescent in the solid state and also show remarkable turn-on of luminescence upon induced aggregation in 1,4-dioxane/water mixtures. While for the *gem*-diphenyl ethenylene-substituted furo[2,3-*c*]isoquinoline, this increase of luminescence can be clearly considered as aggregation-induced emission enhancement, fluorenylidene-expanded furo[2,3-*c*]isoquinolines rather display typical AIE behaviour, with green over yellow to orange-red luminescence in the induced aggregates, some with quite remarkable fluorescence quantum yields. The excitation–relaxation–emission–relaxation cycle of the *gem*-diphenyl ethenylene-substituted furo[2,3-*c*]isoquinoline and the parent fluorenylidene furo[2,3-*c*]isoquinoline dye is well reproduced by TD-DFT calculations for rationalizing the observed emission in solution.

Author contributions

Synthesis of the molecules: T. C.: methodology, validation investigation, and data curation. A. M.: validation, investigation, and data curation. L. M.: methodology, data curation, writing – review & editing, and supervision. C. L.: methodology, data curation, and supervision. R. R.: conceptualization, writing – original draft, review & editing, visualization, and supervision. Photophysics: L. B.: investigation, validation,

formal analysis, visualization, and data curation. Quantum chemical calculations: B. M.: methodology, investigation, validation, visualization, and data curation. T. J. J. M.: conceptualization, writing – original draft, review & editing, visualization, supervision, funding acquisition, and project administration. All authors have read and agreed to the published version of the manuscript.

Conflicts of interest

There are no conflicts to declare.

Data availability

The data supporting this article have been included as part of the supplementary information (SI). Supplementary information is available (Synthetic approach to compounds **8a–n**, Experimental procedures, Additional information on Photophysics and Computation, Copies of ^{1}H and ^{13}C spectra). See DOI: **https://doi.org/10.1039/d6qo00311g**.

Acknowledgements

The University of Genova is kindly acknowledged for the contribution to the acquisition of an NMR instrument. The authors acknowledge Dr Daniele di Stefano and Dr Sergio Mulone for performing some preliminary experiments and Dr Walter Sgroi for his collaboration for IR spectra recording. The authors are grateful to the Deutsche Forschungsgemeinschaft DFG (Mu 1088/9-1) and the Fonds der Chemischen Industrie for financial support. We also thank the Centre for Information and Media Technology (ZIM) for the opportunity to perform our TD-DFT calculations on the Hilbert high-performance computing cluster.

References

1 M. Guerre, C. Taplan, J. M. Winne and F. E. Du Prez, Vitrimers: Directing Chemical Reactivity to Control Material Properties, *Chem. Sci.*, 2020, **11**, 4855–4870.
2 B. Roy, M. C. Reddy and P. Hazra, Developing the Structure–Property Relationship to Design Solid State Multi-Stimuli Responsive Materials and Their Potential Applications in Different Fields, *Chem. Sci.*, 2018, **9**, 3592–3606.
3 K. W. Moore, A. Pechen, X.-J. Feng, J. Dominy, V. Beltrani and H. Rabitz, Universal Characteristics of Chemical Synthesis and Property Optimization, *Chem. Sci.*, 2011, **2**, 417–424.
4 J. Griffiths, The Functional Dyes – Definition, Design, and Development, *Chimia*, 1991, **45**, 304–307.
5 H. Ogasawara, Y. Tanaka, M. Taki and S. Yamaguchi, Late-Stage Functionalisation of Alkyne-Modified Phospha-Xanthene Dyes: Lysosomal Imaging Using an Off-on-Off Type of pH Probe, *Chem. Sci.*, 2021, **12**, 7902–7907.
6 Y. Ooyama and Y. Harima, Photophysical and Electrochemical Properties, and Molecular Structures of Organic Dyes for Dye-Sensitized Solar Cells, *ChemPhysChem*, 2012, **13**, 4032–4080.
7 A. Alagumalai, M. K. Munavvar Fairoos, P. Vellimalai, M. C. Sil and J. Nithyanandhan, Effect of out-of-Plane Alkyl Group's Position in Dye-Sensitized Solar Cell Efficiency: A Structure-Property Relationship Utilizing Indoline-Based Unsymmetrical Squaraine Dyes, *ACS Appl. Mater. Interfaces*, 2016, **8**, 35353–35367.
8 G. Li, K.-J. Jiang, Y.-F. Li, S.-L. Li and L.-M. Yang, Efficient Structural Modification of Triphenylamine-Based Organic Dyes for Dye-Sensitized Solar Cells, *J. Phys. Chem. C*, 2008, **112**, 11591–11599.
9 X. Jiang, T. Marinado, E. Gabrielsson, D. P. Hagberg, L. Sun and A. Hagfeldt, Structural Modification of Organic Dyes for Efficient Coadsorbent-Free Dye-Sensitized Solar Cells, *J. Phys. Chem. C*, 2010, **114**, 2799–2805.
10 D. Zhao and T. M. Swager, Sensory Responses in Solution Vs Solid State: A Fluorescence Quenching Study of Poly (Iptycenebutadiynylene)S, *Macromolecules*, 2005, **38**, 9377–9384.
11 S. Liu, Y. Cheng, Y. Li, M. Chen, J. W. Y. Lam and B. Z. Tang, Manipulating Solid-State Intramolecular Motion toward Controlled Fluorescence Patterns, *ACS Nano*, 2020, **14**, 2090–2098.
12 M. Taguchi, T. Nakagawa, T. Nakashima and T. Kawai, Photochromic and Fluorescence Switching Properties of Oxidized Triangle Terarylenes in Solution and in Amorphous Solid States, *J. Mater. Chem.*, 2011, **21**, 17425–17432.
13 F. Würthner, Aggregation-Induced Emission (AIE): A Historical Perspective, *Angew. Chem., Int. Ed.*, 2020, **59**, 14192–14196.
14 H. Wang, E. Zhao, J. W. Y. Lam and B. Z. Tang, AIE Luminogens: Emission Brightened by Aggregation, *Mater. Today*, 2015, **18**, 365–377.
15 J. Mei, N. L. Leung, R. T. Kwok, J. W. Lam and B. Z. Tang, Aggregation-Induced Emission: Together We Shine, United We Soar!, *Chem. Rev.*, 2015, **115**, 11718–11940.
16 J. Mei, Y. Hong, J. W. Lam, A. Qin, Y. Tang and B. Z. Tang, Aggregation-Induced Emission: The Whole Is More Brilliant Than the Parts, *Adv. Mater.*, 2014, **26**, 5429–5479.
17 Z. He, C. Ke and B. Z. Tang, Journey of Aggregation-Induced Emission Research, *ACS Omega*, 2018, **3**, 3267–3277.
18 C. Niu, Y. You, L. Zhao, D. He, N. Na and J. Ouyang, Solvatochromism, Reversible Chromism and Self-Assembly Effects of Heteroatom-Assisted Aggregation-Induced Enhanced Emission (AIEE) Compounds, *Chem. – Eur. J.*, 2015, **21**, 13983–13990.
19 J. Xu, J. Wang, O. M. Bakr and N. Hadjichristidis, Controlling the Fluorescence Performance of AIE Polymers by Controlling the Polymer Microstructure, *Angew. Chem., Int. Ed.*, 2023, **62**, e202217418.

20 Y. Zhang, S. Xie, Z. Zeng and B. Z. Tang, Functional Scaffolds from AIE Building Blocks, *Matter*, 2020, **3**, 1862–1892.
21 Y. Tu, Z. Zhao, J. W. Y. Lam and B. Z. Tang, Mechanistic Connotations of Restriction of Intramolecular Motions (RIM), *Natl. Sci. Rev.*, 2021, **8**, nwaa260.
22 N. L. Leung, N. Xie, W. Yuan, Y. Liu, Q. Wu, Q. Peng, Q. Miao, J. W. Lam and B. Z. Tang, Restriction of Intramolecular Motions: The General Mechanism Behind Aggregation-Induced Emission, *Chem. – Eur. J.*, 2014, **20**, 15349–15353.
23 R. Crespo-Otero and L. Blancafort, A Global Potential Energy Surface Approach to the Photophysics of AIEgens, in *Handbook of Aggregation–Induced Emission*, ed. Y. Tang and B.-Z. Tang, Wiley Online Library, 2022, pp. 411–454.
24 X.-L. Peng, S. Ruiz-Barragan, Z.-S. Li, Q.-S. Li and L. Blancafort, Restricted Access to a Conical Intersection to Explain Aggregation Induced Emission in Dimethyl Tetraphenylsilole, *J. Mater. Chem. C*, 2016, **4**, 2802–2810.
25 C. Wang, Z. Liu, M. Li, Y. Xie, B. Li, S. Wang, S. Xue, Q. Peng, B. Chen, Z. Zhao, Q. Li, Z. Ge and Z. Li, The Marriage of AIE and Interface Engineering: Convenient Synthesis and Enhanced Photovoltaic Performance, *Chem. Sci.*, 2017, **8**, 3750–3758.
26 Y. Li, Y. Zhang, X. Zuo and Y. Lin, Organic Photovoltaic Electron Acceptors Showing Aggregation-Induced Emission for Reduced Nonradiative Recombination, *Chem. Commun.*, 2021, **57**, 5135–5138.
27 D. Liu, J. Y. Wei, W. W. Tian, W. Jiang, Y. M. Sun, Z. Zhao and B. Z. Tang, Endowing TADF Luminophors with AIE Properties through Adjusting Flexible Dendrons for Highly Efficient Solution-Processed Nondoped OLEDs, *Chem. Sci.*, 2020, **11**, 7194–7203.
28 L. Yu, Z. Wu, G. Xie, W. Zeng, D. Ma and C. Yang, Molecular Design to Regulate the Photophysical Properties of Multifunctional TADF Emitters Towards High-Performance TADF-Based OLEDs with EQEs up to 22.4% and Small Efficiency Roll-Offs, *Chem. Sci.*, 2018, **9**, 1385–1391.
29 C. Gui, E. Zhao, R. T. K. Kwok, A. C. S. Leung, J. W. Y. Lam, M. Jiang, H. Deng, Y. Cai, W. Zhang, H. Su and B. Z. Tang, AIE-Active Theranostic System: Selective Staining and Killing of Cancer Cells, *Chem. Sci.*, 2017, **8**, 1822–1830.
30 N. Song, Z. Zhang, P. Liu, Y. W. Yang, L. Wang, D. Wang and B. Z. Tang, Nanomaterials with Supramolecular Assembly Based on AIE Luminogens for Theranostic Applications, *Adv. Mater.*, 2020, **32**, e2004208.
31 Z. Yang, W. Qin, J. W. Y. Lam, S. Chen, H. H. Y. Sung, I. D. Williams and B. Z. Tang, Fluorescent pH Sensor Constructed from a Heteroatom-Containing Luminogen with Tunable AIE and ICT Characteristics, *Chem. Sci.*, 2013, **4**, 3725–3730.
32 J. Shi, Q. Deng, C. Wan, M. Zheng, F. Huang and B. Tang, Fluorometric Probing of the Lipase Level as Acute Pancreatitis Biomarkers Based on Interfacially Controlled Aggregation-Induced Emission (AIE), *Chem. Sci.*, 2017, **8**, 6188–6195.
33 S. Chen, J. Liu, Y. Liu, H. Su, Y. Hong, C. K. W. Jim, R. T. K. Kwok, N. Zhao, W. Qin, J. W. Y. Lam, K. S. Wong and B. Z. Tang, An AIE-Active Hemicyanine Fluorogen with Stimuli-Responsive Red/Blue Emission: Extending the pH Sensing Range by "Switch + Knob" Effect, *Chem. Sci.*, 2012, **3**, 1804–1809.
34 D. D. La, S. V. Bhosale, L. A. Jones and S. V. Bhosale, Tetraphenylethylene-Based AIE-Active Probes for Sensing Applications, *ACS Appl. Mater. Interfaces*, 2018, **10**, 12189–12216.
35 R. Riva, L. Moni and T. J. J. Müller, Multicomponent Strategies for the Diversity-Oriented Synthesis of Blue Emissive Heterocyclic Chromophores, in *Targets Heterocycl. Syst*, ed. O. A. Attanasi, P. Merino and D. Spinelli, Società Chimica Italiana, Urbino (I), 2016, vol. 20, pp. 85–112.
36 L. Levi and T. J. J. Müller, Multicomponent Syntheses of Functional Chromophores, *Chem. Soc. Rev.*, 2016, **45**, 2825–2846.
37 L. Brandner and T. J. J. Müller, Multicomponent Synthesis of Chromophores - the One-Pot Approach to Functional π-Systems, *Front. Chem.*, 2023, **11**, 1124209.
38 L. Levi and T. J. J. Müller, Multicomponent Syntheses of Fluorophores Initiated by Metal Catalysis, *Eur. J. Org. Chem.*, 2016, 2902–2918.
39 T. J. J. Müller, Multi-Component Synthesis of Fluorophores Via Catalytic Generation of Alkynoyl Intermediates, *Drug Discovery Today: Technol.*, 2018, **29**, 19–26.
40 F. K. Merkt and T. J. J. Müller, Solid State and Aggregation Induced Emissive Chromophores by Multi–Component Syntheses, *Isr. J. Chem.*, 2018, **58**, 889–900.
41 U. K. Sharma, N. Sharma, D. D. Vachhani and E. V. Van der Eycken, Metal-Mediated Post-Ugi Transformations for the Construction of Diverse Heterocyclic Scaffolds, *Chem. Soc. Rev.*, 2015, **44**, 1836–1860.
42 X. Tang, Q. Tao, L. Song and E. V. Van der Eycken, Recent Advances in Post Ugi-4CR Dearomatizations for Constructing Spiro Heterocycles, *Org. Chem. Front.*, 2024, **11**, 4895–4912.
43 L. Moni, M. Denißen, G. Valentini, T. J. J. Müller and R. Riva, Diversity-Oriented Synthesis of Intensively Blue Emissive 3-Hydroxyisoquinolines by Sequential Ugi Four-Component Reaction/Reductive Heck Cyclization, *Chem. – Eur. J.*, 2015, **21**, 753–762.
44 L. Moni, C. F. Gers-Panther, M. Anselmo, T. J. J. Müller and R. Riva, Highly Convergent Synthesis of Intensively Blue Emissive Furo[2,3-*c*]Isoquinolines by a Palladium-Catalyzed Cyclization Cascade of Unsaturated Ugi Products, *Chem. – Eur. J.*, 2016, **22**, 2020–2031.
45 L. Moni, F. Merkt-Tasch, B. Mayer, S. Mulone, T. J. J. Müller and R. Riva, Luminescent Furo[2,3-*c*]Isoquinolines as Fluorophores - Tuning the Luminophore by Donor Substitution, *Dyes Pigm.*, 2023, **214**, 111190.
46 M. J. Frisch, G. W. Trucks, H. B. Schlegel, G. E. Scuseria, M. A. Robb, J. R. Cheeseman, G. Scalmani, V. Barone, G. A. Petersson, H. Nakatsuji, X. Li, M. Caricato, A. V. Marenich, J. Bloino, B. G. Janesko, R. Gomperts,

B. Mennucci, H. P. Hratchian, J. V. Ortiz, A. F. Izmaylov, J. L. Sonnenberg, D. Williams-Young, F. Ding, F. Lipparini, F. Egidi, J. Goings, B. Peng, A. Petrone, T. Henderson, D. Ranasinghe, V. G. Zakrzewski, J. Gao, N. Rega, G. Zheng, W. Liang, M. Hada, M. Ehara, K. Toyota, R. Fukuda, J. Hasegawa, M. Ishida, T. Nakajima, Y. Honda, O. Kitao, H. Nakai, T. Vreven, K. Throssell, J. A. Montgomery Jr., J. E. Peralta, F. Ogliaro, M. J. Bearpark, J. J. Heyd, E. N. Brothers, K. N. Kudin, V. N. Staroverov, T. A. Keith, R. Kobayashi, J. Normand, K. Raghavachari, A. P. Rendell, J. C. Burant, S. S. Iyengar, J. Tomasi, M. Cossi, J. M. Millam, M. Klene, C. Adamo, R. Cammi, J. W. Ochterski, R. L. Martin, K. Morokuma, O. Farkas, J. B. Foresman and D. J. Fox, *Gaussian 16, Revision A.03*, Gaussian, Inc., Wallingford CT, 2016.

47 C. Lee, W. Yang and R. G. Parr, Development of the Colle-Salvetti Correlation-Energy Formula into a Functional of the Electron Density, *Phys. Rev. B: Condens. Matter Mater. Phys.*, 1988, **37**, 785–789.

48 A. D. Becke, A New Mixing of Hartree–Fock and Local Density-Functional Theories, *J. Chem. Phys.*, 1993, **98**, 1372–1377.

49 A. D. Becke, Density-Functional Thermochemistry., III. The Role of Exact Exchange, *J. Chem. Phys.*, 1993, **98**, 5648–5652.

50 K. Kim and K. D. Jordan, Comparison of Density Functional and MP2 Calculations on the Water Monomer and Dimer, *J. Phys. Chem.*, 1994, **98**, 10089–10094.

51 P. J. Stephens, F. J. Devlin, C. F. Chabalowski and M. J. Frisch, Ab Initio Calculation of Vibrational Absorption and Circular Dichroism Spectra Using Density Functional Force Fields, *J. Phys. Chem.*, 2002, **98**, 11623–11627.

52 R. Krishnan, J. S. Binkley, R. Seeger and J. A. Pople, Self-Consistent Molecular Orbital Methods. XX. A Basis Set for Correlated Wave Functions, *J. Chem. Phys.*, 1980, **72**, 650–654.

53 M. Caricato, B. Mennucci, J. Tomasi, F. Ingrosso, R. Cammi, S. Corni and G. Scalmani, Formation and Relaxation of Excited States in Solution: A New Time Dependent Polarizable Continuum Model Based on Time Dependent Density Functional Theory, *J. Chem. Phys.*, 2006, **124**, 124520.

54 G. Scalmani and M. J. Frisch, Continuous Surface Charge Polarizable Continuum Models of Solvation. I. General Formalism, *J. Chem. Phys.*, 2010, **132**, 114110.

55 A. Dreuw and M. Head-Gordon, Failure of Time-Dependent Density Functional Theory for Long-Range Charge-Transfer Excited States: The Zincbacteriochlorin-Bacteriochlorin and Bacteriochlorophyll-Spheroidene Complexes, *J. Am. Chem. Soc.*, 2004, **126**, 4007–4016.

56 J. D. Chai and M. Head-Gordon, Long-Range Corrected Hybrid Density Functionals with Damped Atom-Atom Dispersion Corrections, *Phys. Chem. Chem. Phys.*, 2008, **10**, 6615–6620.

57 R. Baer and D. Neuhauser, Density Functional Theory with Correct Long-Range Asymptotic Behavior, *Phys. Rev. Lett.*, 2005, **94**, 043002.

58 E. Runge and E. K. U. Gross, Density-Functional Theory for Time-Dependent Systems, *Phys. Rev. Lett.*, 1984, **52**, 997–1000.

59 D. Jacquemin, E. A. Perpete, I. Ciofini and C. Adamo, Accurate Simulation of Optical Properties in Dyes, *Acc. Chem. Res.*, 2009, **42**, 326–334.

60 C. Adamo and D. Jacquemin, The Calculations of Excited-State Properties with Time-Dependent Density Functional Theory, *Chem. Soc. Rev.*, 2013, **42**, 845–856.